Isotropic−Nematic Interface in a Lyotropic System of Wormlike Chains with the Onsager Interaction

Ying Jiang and Jeff Z. Y. Chen*

Guelph-Waterloo Physics Institute, and Department of Physics and Astronomy, University of Waterloo, Waterloo, Ontario, Canada N2L 3G1

Received October 5, 2010; Revised Manuscript Received November 5, 2010

ABSTRACT: The effects of the flexibility of constituent wormlike chains on the interfacial properties between isotropic and nematic phases are investigated in a self-consistent mean-field approximation. The model is built from a wormlike chain formalism which crosses over from the rod limit to the flexible limit, and the Onsager-type interaction which describes the orientation-dependent repulsive interaction. Physical properties such as the surface tension, interfacial width, and density- and order-parameter profiles are numerically calculated as functions of varying flexibility (defined as the ratio between the total polymer length and the persistent length) and tilt angle (defined as the angle between the interfacial normal and the nematic director in the nematic phase). The resulting modified diffusion equation is numerically solved by using a combination of the Crank−Nicolson algorithm and SPHEREPACK, a software package that deals with the analysis and synthesis of spherical-harmonics functions.

1. Introduction

The spacial variation of an isotropic−nematic interface is closely coupled with the orientational properties of constituent molecules, microscopically; in comparison with the interface produced in a small-molecule system where the orientational degrees of freedom of a molecule can be ignored, an isotropic−nematic interface also macroscopically depends on the angle that the interfacial normal makes with respect to the nematic director far away on the liquid-crystal side. Models of the isotropic−nematic interface in liquid crystals consisting of semiflexible, interacting polymer chains have been actively studied by theoretical work[1−11] in recent years, and related experimental work in colloids,[12,13] tactoidal droplets,[14,15] and viruses[16,17] have been reported as well.

The flexibility of a wormlike polymer chain can be described by the ratio between the total chain length L and the persistence length λ. Past theoretical studies of a polymeric liquid-crystal interface mostly focused on the limit of a rigid, rodlike system ($L \ll \lambda$) where the rod length L is a characteristic length scale,[1,2,5,8,9,18] or the limit of a flexible system ($L \gg \lambda$) where the persistence length λ plays a dominating role;[3,10] in these two limits, theoretical treatments can be somewhat simplified. Experimental measurements can be done in systems where the chain length may be changed but the persistence length is kept fixed.[13] The effects of semiflexibility on a polymeric liquid-crystal interface remain theoretically unexplored.

A theoretically well-defined model for a liquid crystal consisting of lyotropic wormlike polymer chains can be traced back to the classical work of Onsager.[19] In such a system, a polymer chain can be modeled by a cylindrical filament (a microscopic version of a garden hose) where the diameter d characterizes the self-avoiding nature between different polymer segments. In a lyotropic case, the orientational dependence of the excluded-volume interaction is responsible for driving the system to form a nematic

phase in relatively high densities, as originally discussed by Onsager[19] for rigid rods, and latter generalized to wormlike polymers by Khokhlov, Semenov,[20] and Grosberg.[21] The bulk properties, for example, dependencies of the transition densities, orientational order parameter, and free-energy related properties such as the chemical potential and osmotic pressure on the flexibilty L/λ, are now known through an exact numerical solution to the differential equation yielded from this model.[22]

This paper examines the influence of the flexibility on the isotropic−nematic interface of a lyotropic polymer system that incorporates the Onsager interaction, for any ratios of L/λ. The only two ingredients in the model are: a statistical description for the wormlike polymer where the ratio L/λ is introduced and the Onsager interaction which drives the isotropic−nematic transition. This interfacial study fills the gap between the limit of $L \ll \lambda$[1,5,9] and the limit of $L \gg \lambda$ previously examined.[3,10] This interfacial study is also an extension to the earlier work on the determination of the isotropic−nematic transition, where the bulk properties were calculated.[22] The results in this paper can be compared with experimental systems where the isotropic−nematic interface is inherently flat, or having curved interface where the curvature is much less than the inverse interface width, to be examined below.

A technical advance in numerical approach is critical to carry out the current calculation. A difficult problem in the self-consistent mean-field treatment of polymer theory is accurately and efficiently solving the resulting modified diffusion equation (MDE) in multiple dimensions. Cui, Akcakir, and Chen considered the solution to MDE of a wormlike chain, expanding the orientational dependence in terms of spherical harmonics and taking a finite difference in the spatial variable;[3] this approach was followed in later work for related systems.[23−26] Matsen suggested solving MDE of a similar type through constructing orthonormal eigenfunctions which describe both spatial and orientational variations, to study the lamellar phase self-assembled by semiflexible diblock copolymers under a periodical boundary condition.[27] Recently, Song et al. developed a numerical method coupling the forward-time and centered-space schemes together with a finite-volume algorithm to solve MDE.[28]

*To whom correspondence should be addressed. E-mail: jeffchen@uwaterloo.ca.

The method used in this paper is similar in spirit to the treatment proposed by Cui et al.;[3] the main difference is that our algorithm utilizes a software package, SPHEREPACK, which provides a fast and efficient spherical−harmonic analysis and synthesis transformations[29] to deal with the orientational dependence; the positional and path variables are treated by the unconditionally stable Crank−Nicolson algorithm. This treatment can be generalized to systems without the type of periodic boundary conditions proposed by Matsen;[27] the method also has the advantage of letting the software package to deal with the mathematical complexities in handling the spherical expansion which no longer requires manual calculations.[3,23]

This paper is organized as follows. In section 2, we introduce the theoretical framework that the current calculation is based on for an arbitrary flexibility. The discussion and proof that this model exactly yields the rod formalism and flexible-chain formalism in the corresponding limits are given in Appendices A and B, respectively. We also discuss the numerical algorithm in detail within this section. In section 3, the main numerical results are given and discussed; readers who do not wish to know the self-consistent mean-field treatment and numerical approaches can directly skip to this section.

2. General Formalism

In this section, we introduce the general formalism yielded from the self-consistent mean-field theory (SCMFT) for a wormlike chain problem that is used for the calculation in this work. We consider a system of volume V consisting of n wormlike homopolymers. Each polymer chain is a cylindrical filament and has a total contour length L and a diameter d. We assume that the configuration of a chain is described by the Saito-Takahashi−Yunoki model,[30] which is a continuous version of the Kratky−Porod model.[31] Mathematically the configuration of a chain is described by a continuous space curve $\mathbf{R}(s)$, where $s \in [0,L]$ is the arc variable along the polymer backbone. The vector $\mathbf{u}(s) \equiv d\mathbf{R}(s)/ds$ specifies the tangent direction at s and is restricted to be a unit vector in our treatment, i.e. $|\mathbf{u}(s)| = 1$.

We are interested in the calculation of the free energy, which is related to the partition function of the system,

$$Z = \frac{1}{n!} \int \prod_{i=1}^{n} \mathcal{D}[R_i] \exp(-\mathcal{H}) \qquad (1)$$

where the Hamiltonian $\mathcal{H}$ consists of two parts: $\mathcal{H} = \mathcal{H}_1 + \mathcal{H}_2$. The first part is the bending energy of wormlike chains,

$$\mathcal{H}_1 = \frac{\lambda}{2} \sum_{i=1}^{n} \int_0^L ds \left| \frac{d\mathbf{u}_i(s)}{ds} \right|^2 \qquad (2)$$

The microscopic parameter, bare *persistence length* λ, describes the distance along the contour of a wormlike chain over which the orientational correlation exponentially decays. The other part is the Onsager-type excluded-volume interaction potential,[19,20]

$$\mathcal{H}_2 = a^2 d \int d\mathbf{r} \, d\mathbf{u} \, d\mathbf{u}' \, \hat{\rho}(\mathbf{r}, \mathbf{u}') |\mathbf{u} \times \mathbf{u}'| \hat{\rho}(\mathbf{r}, \mathbf{u}) \qquad (3)$$

where a represents the Kuhn length and is related to λ by[30]

$$a = 2\lambda \qquad (4)$$

in the limit of $L \gg \lambda$ for a $d = 0$ polymer in a free space (i.e., $\mathcal{H}_2 = 0$). Here we introduce a segment density operator

$$\hat{\rho}(\mathbf{r}, \mathbf{u}) = \frac{1}{a} \sum_{i=1}^{n} \int_0^L ds \, \delta[\mathbf{r} - \mathbf{R}_i(s)] \delta[\mathbf{u} - \mathbf{u}_i(s)] \qquad (5)$$

which is a function of both $\mathbf{r}$ and $\mathbf{u}$.[32]

Following the SCMFT treatment, where a self-consistent field $W(\mathbf{r}, \mathbf{u})$ is introduced[32] in conjugation to the operator $\hat{\rho}$, we can write the Helmholtz free energy per chain as

$$\frac{F}{k_B T} = \ln\left(\frac{n}{Q}\right) + \frac{a^2 d}{n} \int d\mathbf{r} \, d\mathbf{u} \, d\mathbf{u}' \, \phi(\mathbf{r}, \mathbf{u}) |\mathbf{u}$$
$$\times \mathbf{u}'| \phi(\mathbf{r}, \mathbf{u}') - \frac{1}{n} \int d\mathbf{r} \, d\mathbf{u} \, W(\mathbf{r}, \mathbf{u}) \phi(\mathbf{r}, \mathbf{u}) \qquad (6)$$

The density distribution function $\phi(\mathbf{r}, \mathbf{u})$ is the statistical average of $\hat{\rho}$ and represents the density of segments of length a, satisfying the normalization condition

$$\int d\mathbf{r} \, d\mathbf{u} \, \phi(\mathbf{r}, \mathbf{u}) = nL/a \qquad (7)$$

The partition function of a single chain can be calculated from $Q = \int d\mathbf{r} \int d\mathbf{u} \, q(\mathbf{r}, \mathbf{u}, L)/(4\pi V)$, where the propagator $q(\mathbf{r}, \mathbf{u}, s)$ follows the modified diffusion equation (MDE),

$$\frac{\partial}{\partial s} q(\mathbf{r}, \mathbf{u}, s) = \left[\frac{1}{a} \nabla_{\mathbf{u}}^2 - \mathbf{u} \cdot \nabla - \frac{1}{a} W(\mathbf{r}, \mathbf{u}) \right] q(\mathbf{r}, \mathbf{u}, s) \qquad (8)$$

with the initial condition $q(\mathbf{r}, \mathbf{u}, 0) = 1$.[32] Equations 6−8 were recently considered for the calculation of the structure of a wormlike brush problem by us and co-workers.[33]

For later convenience in this work, we define the reduced variables

$$\overline{\phi}(\mathbf{r}, \mathbf{u}) \equiv \frac{aV}{nL} \phi(\mathbf{r}, \mathbf{u}) \qquad (9)$$

$$\overline{W}(\mathbf{r}, \mathbf{u}) \equiv \frac{L}{a} W(\mathbf{r}, \mathbf{u}) \qquad (10)$$

and

$$\overline{s} \equiv s/L \qquad (11)$$

Note that $\overline{\phi}(\mathbf{r}, \mathbf{u})$ is normalized to V. Then, the free energy per chain can be rewritten as,

$$\frac{F}{k_B T} = \ln\left(\frac{C}{Q}\right) + \frac{1}{V} \int d\mathbf{r} \, d\mathbf{u} \, [C \int d\mathbf{u}' \, \overline{\phi}(\mathbf{r}, \mathbf{u}) |\mathbf{u}$$
$$\times \mathbf{u}'| \overline{\phi}(\mathbf{r}, \mathbf{u}') - \overline{W}(\mathbf{r}, \mathbf{u}) \overline{\phi}(\mathbf{r}, \mathbf{u})] \qquad (12)$$

where a constant shift, $\ln(L^2 d/V)$, in the free energy has been used and

$$C \equiv \frac{nL^2 d}{V} \qquad (13)$$

is the overall reduced chain density in the system. We have kept the same reduction prefactor $L^2 d$ and the symbol C for the chain density following Onsager's original work.[19] We can then rewrite eq 8 using reduced parameters

$$\frac{\partial}{\partial \overline{s}} q(\mathbf{r}, \mathbf{u}, \overline{s}) = [\alpha \nabla_{\mathbf{u}}^2 - L\mathbf{u} \cdot \nabla - \overline{W}(\mathbf{r}, \mathbf{u})] q(\mathbf{r}, \mathbf{u}, \overline{s}) \qquad (14)$$

where the reduced contour variable $\overline{s} \in [0,1]$. The parameter

$$\alpha \equiv L/a \qquad (15)$$

describes the flexibility of a wormlike chain. In the rod-like chain limit $\alpha = 0$ and in the flexible chain limit $\alpha \gg 1$. The current work focuses on how the isotropic−nematic interface is influenced by the flexibility parameter α over the entire range. Minimizing the free energy, eq 12, with respect to the external filed $\overline{W}(\mathbf{r}, \mathbf{u})$ and

density $\bar{\phi}(\mathbf{r},\mathbf{u})$, we obtain equations according to the saddle-point approximation,

$$\overline{\phi}(\mathbf{r},\mathbf{u}) = \frac{1}{4\pi Q} \int_0^1 d\bar{s}\, q(\mathbf{r},\mathbf{u},\bar{s})q(\mathbf{r},-\mathbf{u},1-\bar{s}) \qquad (16)$$

$$\overline{W}(\mathbf{r},\mathbf{u}) = \Lambda + 2C \int d\mathbf{u}'|\mathbf{u} \times \mathbf{u}'|\overline{\phi}(\mathbf{r},\mathbf{u}') \qquad (17)$$

where Λ is a constant which will be defined later. Equations 14, 16 and 17 form a self-consistent set of equations that are numerically solved in the next few sections.

2.1. Bulk Phases and the Isotropic−Nematic Phase Transition. In a spatially homogeneous system, i.e., in a bulk phase, we recover the formalism and results studied earlier by one of us.[22] Dropping the **r** dependence and adding a subscript "b" to the physical quantities considered above, we write the Helmholtz free energy per chain in a simplified form

$$\frac{F}{k_\mathrm{B}T} = \ln\left(\frac{C}{Q_\mathrm{b}}\right) + \int d\mathbf{u}\, [C\int d\mathbf{u}'\, \overline{\phi}_\mathrm{b}(\mathbf{u})|\mathbf{u}$$
$$\times \mathbf{u}'|\overline{\phi}_\mathrm{b}(\mathbf{u}') - \overline{W}_\mathrm{b}(\mathbf{u})\overline{\phi}_\mathrm{b}(\mathbf{u})] \qquad (18)$$

where the partition function of a single chain can be calculated from $Q_\mathrm{b} = 1/(4\pi) \int d\mathbf{u}\, q_\mathrm{b}(\mathbf{u},\bar{s}=1)$. The free energy [eq 18], together with the MDE [eq 14 without the $\mathbf{u}\cdot\nabla$ term], was considered earlier,[22] where the isotropic-nematic transition for any chain flexibility α was determined. We verify this result in this section.

In our lyotropic system, at a given flexibility parameter α, the only parameter that controls the physical properties of the system is the reduced density C. At the first-order isotropic−nematic phase transition, the chemical potentials calculated from the isotropic density C_i and the nematic density C_n are equal, $\mu(C_\mathrm{i}) = \mu(C_\mathrm{n})$; the osmotic pressures are equal as well, $P(C_\mathrm{i}) = P(C_\mathrm{n})$. Both the chemical potential and osmotic pressure can be calculated from the free energy in the above, by $\mu \equiv [\partial(nF)/\partial n]_{T,V}$ and $P \equiv -[\partial(nF)/\partial V]_{T,n}$ once the reduced density is specified.[20,22,34,35] The two phase-balancing equations are nonlinear in C_i and C_n; we use the Newton−Raphson algorithm[36] to solve this set of nonlinear equations to determine C_i and C_n.

The calculation of the free energy requires an accurate computational algorithm to solve the MDE. In a bulk phase, eq 14 is reduced to

$$\frac{\partial}{\partial\bar{s}} q_\mathrm{b}(\mathbf{u},\bar{s}) = [\alpha\nabla_\mathbf{u}^2 - \overline{W}_\mathrm{b}(\mathbf{u})]q_\mathrm{b}(\mathbf{u},\bar{s}) \qquad (19)$$

with the initial condition $q_\mathrm{b}(\mathbf{u},0) = 1$. Chantawansri et al. introduced a software package, SPHEREPACK, to successfully deal with the two-dimensional Laplacian operator $\nabla_\mathbf{u}^2$ on the surface of a unit sphere in the study of diblock copolymer self-assembly on a sphere with chain statistics described by the Gaussian model.[37] SPHEREPACK promises to provide an efficient spherical harmonic analysis and synthesis transformation[38] and was developed by Adams and Swarztrauber of the National Center for Atmospheric Research.[29] Subroutines written in FORTRAN 77 are available for implementing the fast Fourier transform (FFT) on the azimuthal angle $\varphi \in [0,2\pi)$ and either equally spaced or Gauss-distributed grid points on the polar angle $\theta \in [0,\pi]$.[39] The subroutines treat function transformations in real number, which save half computation time compared to those using complex numbers on scalar spherical harmonic functions.[40]

We have implemented SPHEREPACK in our treatment of the operator $\nabla_\mathbf{u}^2$.

Our treatment of the $\partial/\partial\bar{s}$ operator followed the unconditionally stable Crank−Nicolson algorithm.[36] Introducing a contour step $\Delta\bar{s}$ for $\bar{s}$, we solved eq 19 in the form of

$$\left[1 - \frac{\alpha\Delta\bar{s}}{2}\nabla_\mathbf{u}^2\right]q_b(\mathbf{u},\bar{s}+\Delta\bar{s})$$
$$= \frac{1-(\Delta\bar{s}/2)\overline{W}_b(\mathbf{u})}{1+(\Delta\bar{s}/2)\overline{W}_b(\mathbf{u})}\left[1 + \frac{\alpha\Delta\bar{s}}{2}\nabla_\mathbf{u}^2\right]q_b(\mathbf{u},\bar{s}) \qquad (20)$$

The entire numerical procedure proceeds as follows, starting from a known $q_\mathrm{b}(\mathbf{u},\bar{s})$ at step $\bar{s}$. We utilized the analysis and synthesis transformation of SPHEREPACK[29] to calculate $\nabla_\mathbf{u}^2 q_\mathrm{b}(\mathbf{u},\bar{s})$. As the next step, we used the analysis transform again on the right side of eq 20, defined as a new function $f(\mathbf{u},\bar{s})$; we then consider

$$f(\mathbf{u},\bar{s}) = \sum_{l=0}^{\overline{L}}\sum_{m=0}^{l} P_l^m(\cos\theta)[a_{l,m}(\bar{s})\cos(m\varphi)$$
$$+ b_{l,m}(\bar{s})\sin(m\varphi)] \qquad (21)$$

where $P_l^m(\cos\theta)$ is the Legendre polynomial and the integer $\overline{L}$ controls the precision of the transform. Finally, we set

$$c_{l,m}(\bar{s}+\Delta\bar{s}) = a_{l,m}(\bar{s})\left[1 + \frac{\alpha\Delta\bar{s}}{2}l(l+1)\right]^{-1} \qquad (22)$$

$$d_{l,m}(\bar{s}+\Delta\bar{s}) = b_{l,m}(\bar{s})\left[1 + \frac{\alpha\Delta\bar{s}}{2}l(l+1)\right]^{-1} \qquad (23)$$

to calculate

$$q_b(\mathbf{u},\bar{s}+\Delta\bar{s}) = \sum_{l=0}^{\overline{L}}\sum_{m=0}^{l} P_l^m(\cos\theta)[c_{l,m}(\bar{s}+\Delta\bar{s})\cos(m\varphi)$$
$$+ d_{l,m}(\bar{s}+\Delta\bar{s})\sin(m\varphi)] \qquad (24)$$

with the assistance of a synthesis transformation.

In our current numerical calculation, we used evenly spaced grid points in both $\theta \in [0,\pi]$ and $\varphi \in [0,2\pi)$, broken into N_θ and N_φ slabs, respectively. In a bulk phase, for the nematic phase, the function $q_b(\mathbf{u},\bar{s})$ has no φ dependence due to axial symmetry about the nematic director. The φ dependence in the above algorithm was used for testing the precision of the numerical results in the inhomogeneous case presented below, where the φ dependence becomes important. Taking $\Delta\bar{s} = 0.0002$, $N_\theta = 36$, $N_\varphi = 72$ (and in another comparative study, $N_\theta = 72$, $N_\varphi = 144$), we have calculated the physical properties at the isotropic−nematic phase transition, including the segment density $C_\mathrm{i}(\alpha)$, the nematic segment density of $C_\mathrm{n}(\alpha)$, and the nematic order parameter $S_2 \equiv \langle P_2(\cos\theta)\rangle$, which are shown as functions of the flexibility parameter α in Figure 1. Our results of $C_\mathrm{i}(\alpha = 0) = 4.1963$, $C_\mathrm{n}(\alpha = 0) = 5.3343$ and $S_2(\alpha = 0) = 0.7902$ fully agree with the results from a number of previous studies.[22,34,35] In the large α limit of Figure 1A,B, we have also added dashed lines representing $C_\mathrm{i}(\alpha \gg 1) = 13.05\alpha$ and $C_\mathrm{n}(\alpha \gg 1) = 14.08\alpha$, which agree well with previous results.[22,41] In the intermediate region of α, our numerical data fully agree with those in ref 22, in which a finite-difference scheme is used to solve eq 19, rather than the
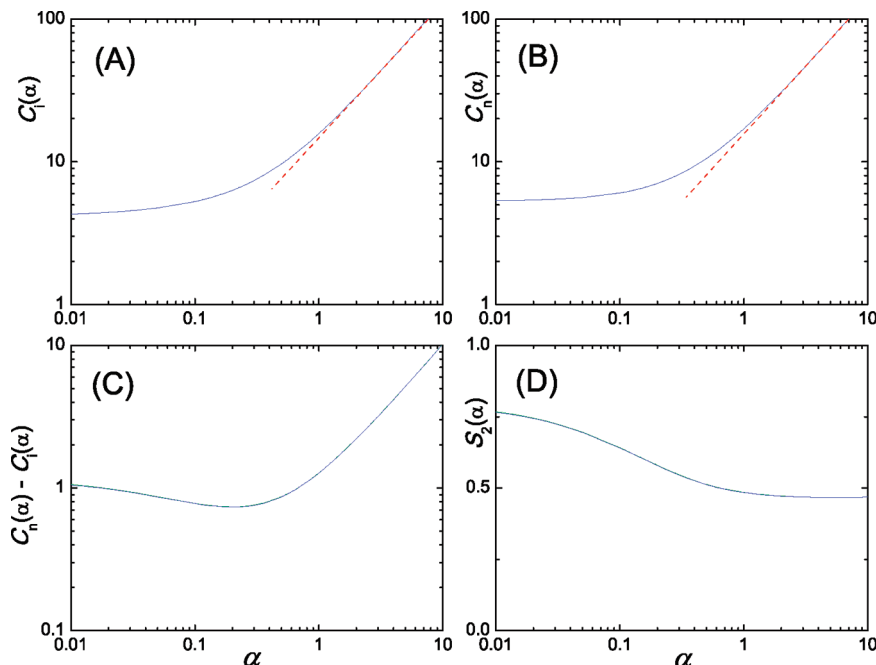
Figure 1. (A) Reduced segment density of the isotropic phase C_i, (B) reduced segment density of the nematic phase C_n, (C) the difference $C_n - C_i$, and (D) orientational order parameter S_2 at the isotropic−nematic phase transition as functions of the flexibility parameter $\alpha \equiv L/a$. Our results of $C_i(\alpha=0) = 4.1963$, $C_n(\alpha=0)=5.3343$ and $S_2(\alpha=0)=0.7902$ and agree with previous results as well.[22,34,35] We have also added dashed lines to plots A and B, which represent $C_i(\alpha \gg 1) = 13.0495\alpha$ and $C_n(\alpha \gg 1) = 14.0769\alpha$ and agree with previous results as well.[22,41]

current use of SPHEREPACK. The precision of our calculation can be described by the difference of calculated properties in two runs: those with $N_\theta = 36$, $N_\varphi = 72$ versus those with $N_\theta = 72$, $N_\varphi = 144$. The difference is not visually identifiable when plotted in Figure 1.

2.2. Isotropic−Nematic Interface: Spatially Inhomogeneous Case. The main task of this work is the study of the isotropic−nematic interface, where the structure described by the segmental density distribution function varies from an isotropic state to a nematic state smoothly. The presence of the interface destroys the rotational symmetry of ϕ about the nematic director; the propagator q needs to be treated with complete dependencies on the spatial variable $\mathbf{r}$, arc variables s, polar angle θ, and azimuthal angle φ, calculated from eq 14.

It turns out that not all three components of $\mathbf{r}$ are needed to describe the system with a flat interface. Considering the coordinate system shown in Figure 2, we assume that the isotropic−nematic interface is in the $y−z$ plane near $x=0$, so that the physical properties vary as functions of x and $\mathbf{u}$ only. As previously noted,[1,3,8] the direction of the nematic director of the nematic phase to the right of the $x=0$ plane, $\mathbf{u}_z$, should be treated as an independent parameter in the system. The unit vector $\mathbf{u}$ is specified in the $\mathbf{u}$ space, where $\mathbf{u}_z$ makes an tilt angle θ_t with respect to the x axis. With the definition of the coordinate system where $\mathbf{u}_y$ coincides with the y-axis, the polar angle θ can be defined from $\cos\theta = \mathbf{u} \cdot \mathbf{u}_z$ and azimuthal angle φ from $\sin\theta \cos\varphi = \mathbf{u} \cdot \mathbf{u}_x$.

Across the entire x-space, the chemical potential per chain μ remains as a constant. This allows us to define a grand thermodynamic potential, $\Xi = nF - n\mu$, in a reduced form,

$$\frac{\Xi Ld}{k_B TAC} = -\bar{\mu} \int d\bar{x}\, d\mathbf{u}\, \bar{\phi}(\bar{x},\mathbf{u}) + \ln\left(\frac{C}{Q}\right) \int d\bar{x}\, d\mathbf{u}\, \bar{\phi}(\bar{x},\mathbf{u})$$

$$- \int d\bar{x}\, d\mathbf{u}\, \overline{W}(\bar{x},\mathbf{u})\bar{\phi}(\bar{x},\mathbf{u}) + C \int d\bar{x}\, d\mathbf{u}\, d\mathbf{u}'\, \bar{\phi}(\bar{x},\mathbf{u})|\mathbf{u}$$

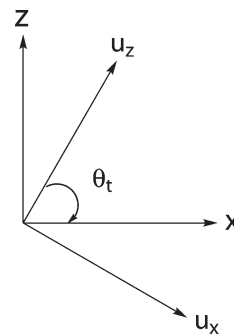$$\times \mathbf{u}'|\bar{\phi}(\bar{x},\mathbf{u}') \qquad (25)$$

Figure 2. Schematic coordinate system. The interface normal is along the x direction and the bulk nematic director is along the $\mathbf{u}_z$ direction, which defines the reference director for the unit vector $\mathbf{u}$. The tilt angle θ_t is defined to be the angle between the x-axis and $\mathbf{u}_z$. The spatial direction y coincides with $\mathbf{u}_y$, both pointing into paper.

where A is the area of the flat interface, $\bar{\mu} \equiv \mu/k_BT$, and the spatial variable is rescaled by

$$\bar{x} \equiv x/L \qquad (26)$$

The partition function of a single chain can be calculated from $Q = \int d\bar{x} \int d\mathbf{u}\, q(\bar{x},\mathbf{u},1)/[4\pi \int d\bar{x} d\mathbf{u}\, \bar{\phi}(\bar{x},\mathbf{u})]$.

Using the coordinate system in Figure 2, we rewrite eq 14 as

$$\frac{\partial}{\partial \bar{s}} q(\bar{x},\mathbf{u},\bar{s})$$

$$= \left[\alpha \nabla_\mathbf{u}^2 - (\cos\theta_t u_z + \sin\theta_t u_x)\frac{\partial}{\partial \bar{x}} - \overline{W}(\bar{x},\mathbf{u})\right] q(\bar{x},\mathbf{u},\bar{s})$$

$$(27)$$

where $u_x = \mathbf{u} \cdot \mathbf{u}_x = \sin\theta \cos\varphi$ and $u_z = \mathbf{u} \cdot \mathbf{u}_z = \cos\theta$. The self-consitent field is given by

$$\overline{W}(\bar{x},\mathbf{u}) = \Lambda + 2C \int d\mathbf{u}'\, |\mathbf{u} \times \mathbf{u}'|\bar{\phi}(\bar{x},\mathbf{u}') \qquad (28)$$
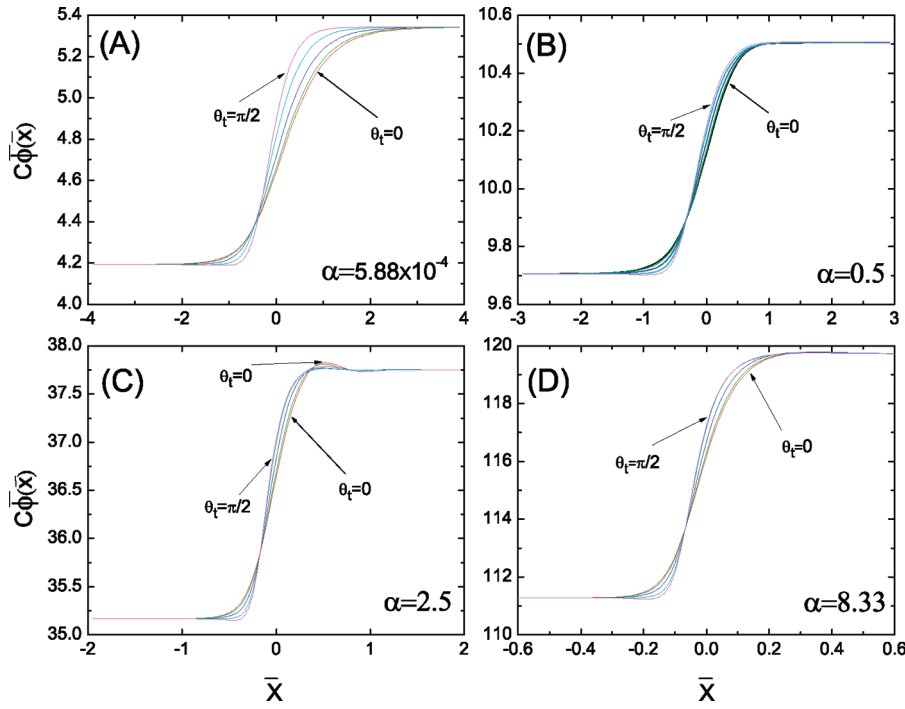
Figure 3. Density profile $C\bar{\phi}(\bar{x})$ of the isotropic−nematic interface as a function of $\bar{x} \equiv x/L$ with a few typical values of the tilt angle θ_t for different flexibility of wormlike chain, (A) $\alpha = 5.88 \times 10^{-4}$, (B) $\alpha = 0.5$, (C) $\alpha = 2.5$, and (D) $\alpha = 8.33$. Red, green, blue, cyan, and pink curves represent $\theta_t = 0, \pi/9, 2\pi/9, \pi/3$, and $\pi/2$, respectively.

from minimization of eq 25 with respect to $\bar{\phi}(\bar{x}, \mathbf{u})$. Note that we have used a constant $\Lambda = 1 - \mu + \ln(C/Q)$ in the actual calculation.

We now illustrate the numerical method used to solve eq 27, using the notations $\hat{F}_1 \equiv -(\cos\theta_t u_z + \sin\theta_t u_x)(\partial/\partial\bar{x}) - \overline{W}(\bar{x}, \mathbf{u})$ and $\hat{F}_2 \equiv \alpha\nabla_{\mathbf{u}}^2$. According to the Crank-Nicolson algorithm, we can decouple the numerical process of solving $q(\bar{x}, \mathbf{u}, \bar{s})$ into two steps

$$\left[1 - \frac{\Delta\bar{s}}{2}\hat{F}_1\right]q(\bar{x}, \mathbf{u}, \bar{s} + \Delta\bar{s}/2) = \left[1 + \frac{\Delta\bar{s}}{2}\hat{F}_2\right]q(\bar{x}, \mathbf{u}, \bar{s}) \quad (29)$$

$$\left[1 - \frac{\Delta\bar{s}}{2}\hat{F}_2\right]q(\bar{x}, \mathbf{u}, \bar{s} + \Delta\bar{s}) = \left[1 + \frac{\Delta\bar{s}}{2}\hat{F}_1\right]q(\bar{x}, \mathbf{u}, \bar{s} + \Delta\bar{s}/2) \quad (30)$$

At the first step, the intermediate $q(\bar{x}, \mathbf{u}, \bar{s} + \Delta\bar{s}/2)$ is obtained through solving the linear set of equations[36] because of the *tridiagonal* matrix property of the operator $1 - (\Delta\bar{s}/2)\hat{F}_1$ for the spatial variable $\bar{x}$. At the second step, similar to the processes described by eqs 21−24 used to solve eq 19, $q(x, \mathbf{u}, \bar{s} + \Delta\bar{s})$ can also be calculated directly from eq 30. Notably, eqs 29 and 30 can be reduced into eq 20 if the propagator q is independent of $\bar{x}$. Once the properties at the step $\bar{s} + \Delta\bar{s}$ are known we go back to eqs 29 and 30 for the next iteration. The chemical potential μ is determined from the phase balancing condition in section 2.1 and can be related to C_i in Figure 1A by $\mu = \ln C_i + (\pi C_i/2) + 1$.

The interface profile changes more drastically at the center and varies more smoothly farther away. Using a rescaled spatial variable $\xi(\bar{x}) \equiv \tanh(\bar{x}/\eta)$ instead of $\bar{x}$ to describe the isotropic−nematic interface,[3] we can effectively place more grid points near the interface by evenly dividing the ξ space. Then, the spatial differential operator in eq 27 can be rewritten as $\partial/\partial\bar{x} = [(1 - \xi^2)/\eta](\partial/\partial\xi)$, where the parameter η was manually adjusted to approximately match the interfacial width. Note that the interval $\bar{x} \in [-\infty, \infty]$ now becomes $\xi \in [-1, 1]$ accordingly. We use $n_\xi = 51$ equally spaced discrete points in the interval $[-1, 1]$, i.e., $\Delta\xi = 0.04$.

The self-consistent calculation started with an initial guess for the self-consistent field $\overline{W}(\bar{x}, \mathbf{u})$, taken as a step function where $\overline{W}(\bar{x}, \mathbf{u}) = 0$ to the left of $x = 0$ and $\overline{W}(\bar{x}, \mathbf{u}) = \overline{W}_b(\mathbf{u})$ (a result from the bulk calculation) to the right. The Picard iteration method used in our previous study of a wormlike chain brush[33] was utilized to update the $\overline{W}(\bar{x}, \mathbf{u})$ function iteratively step-by-step. At every iteration step, a function of $N_\xi \times N_\theta \times N_\varphi \times N_{\bar{s}} = 51 \times 36 \times 72 \times 5001 = 6.61 \times 10^8$ variables was calculated through eq 27. The iteration continued until the convergence criterion imposed on the field was met, $\text{MAX}|\overline{W}^{new}(\bar{x}, \mathbf{u}) - \overline{W}^{old}(\bar{x}, \mathbf{u})| < 10^{-3}$.

3. Results and Discussion

In this section, we discuss the main results obtained from a numerical solution to the SCMFT presented in the last section. The orientational ordering of the polymer segments is normally considered by a traceless matrix.[42] This matrix is a function of the spatial variable $\bar{x}$ across the interface and can be calculated from the statistical average of the tensor $(3\mathbf{uu} - \mathbf{I})/2$

$$\mathbf{S}(\bar{x}) \equiv \frac{1}{2}\frac{\int d\mathbf{u}(3\mathbf{uu} - \mathbf{I})\bar{\phi}(\bar{x}, \mathbf{u})}{\int d\mathbf{u}\bar{\phi}(\bar{x}, \mathbf{u})} \quad (31)$$

It has been noted before[3] that the principal nematic director changes across the isotropic−nematic interface. Mathematically the principal order parameter $S(\bar{x})$ and the biaxiality parameter $P(\bar{x})$ can be found from the diagonalization of the above matrix,[3]

$$\mathscr{U}^{-1}\mathbf{S}(\bar{x})\mathscr{U} = \begin{bmatrix} S(\bar{x}) & 0 & 0 \\ 0 & \frac{1}{2}(P(\bar{x}) - S(\bar{x})) & 0 \\ 0 & 0 & -\frac{1}{2}(P(\bar{x}) - S(\bar{x})) \end{bmatrix}$$

where $\mathscr{U}$ is a 3×3 unitary matrix.

For a number of representative values of α, the profiles of the segmental density $C\bar{\phi}(\bar{x})$, the order parameter $S(\bar{x})$, and the
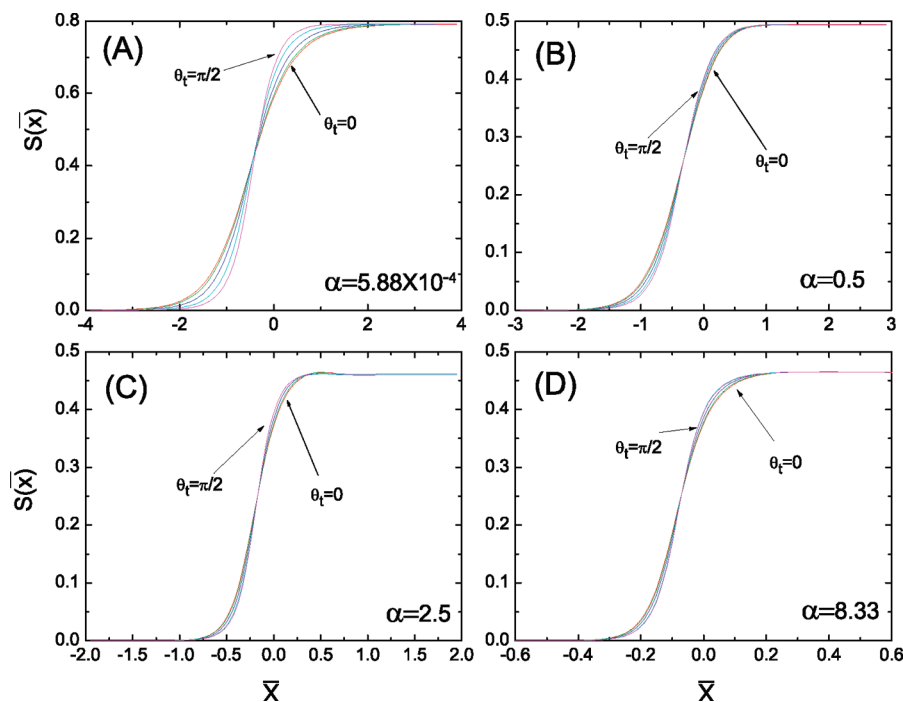
Figure 4. Order parameter profile $S(\overline{x})$ of the isotropic−nematic interface as a function of $\overline{x} \equiv x/L$ with a few typical values of tilt angle θ_t for different flexibility of wormlike chain, (A) $\alpha = 5.88 \times 10^{-4}$, (B) $\alpha = 0.5$, (C) $\alpha = 2.5$, and (D) $\alpha = 8.33$. Red, green, blue, cyan, and pink curves represent the tilt angle $\theta_t = 0$, $\pi/9$, $2\pi/9$, $\pi/3$, and $\pi/2$, respectively.

biaxiality $P(\overline{x})$ are plotted as functions of $\overline{x}$ in Figure 3−5. Within each plot, we have further displayed curves for a few typical values of the tilt angle θ_t. Both $C\overline{\phi}(\overline{x})$ and $S(\overline{x})$ display a narrowest interfacial width when $\theta_t = \pi/2$ and a widened interfacial width as θ_t decreases. A comparison between Figure 3 and Figure 4 reveals that the variation of the density function slightly moves toward the nematic side in comparison with the variation of the order-parameter profile. In all cases, the density profiles show a depletion before entering into the interface from the isotropic side. The density profiles for most values of α increase smoothly to the values at the nematic side, except for intermediate values of α; an example can be seen in Figure 3C where the density profiles are enhanced before entering into the nematic state on the right-hand side, when $\alpha = 2.5$. Correspondingly, a similar enhancement of orientational ordering can be found in Figure 4C.

Figure 5A shows a weak but significant biaxiality across the interface. In the $\theta_t = \pi/2$ case, $P(\overline{x})$ varies more drastically because of the anchoring effect. $\theta_t = 0$ is an interesting case where $P(\overline{x})$ reduces to zero across the entire region; the system actually recovers an axial symmetry about the nematic director in the far right-hand side. Another feature in this figure is the reduction of the magnitude of the biaxiality as α increases—a more flexible polymer can make an easier structural change to facilitate the crossover from the isotropic to nematic sides.

The interfacial tension is normally defined as the interface excess free energy per area, in comparison to that in a bulk phase. For this purpose we define the interfacial tension,

$$\sigma \equiv (\Xi - \Xi_{\text{isotropic}})/A \tag{32}$$

In reduced symbols, this can be calculated from

$$\frac{\sigma L d}{k_{\text{B}} T} = -\int d\overline{x} \left\{ \int d\mathbf{u} \ C\overline{\phi}(\overline{x}, \mathbf{u}) \left[\frac{1}{2} \overline{W}(\overline{x}, \mathbf{u}) + 1 \right] \right.$$

$$\left. + C_i \left[\ln C_i + \frac{\pi C_i}{4} - \overline{\mu} \right] \right\} \tag{33}$$

where it should be understood that eq 28 was used to reduce the longer version in eq 25: the minimization of the free energy with respect to the density profile has already been considered. The term associated with the second set of square brackets in the above expression is the negative osmotic pressure of the isotropic phase; subtracting a reference Ξ by using the nematic Ξ works as well, because this term is identical to $\Xi_{\text{isotropic}}$. The term associated with the first set of brackets can be regarded as the osmotic pressure at the position $\overline{x}$. The entire expression can also be considered as the reduced work performed (per unit area) to move polymer segments from $x = -\infty$, overcoming the osmotic pressure difference, to construct an isotropic−nematic interface.

Figure 6 shows the dependence of interfacial tension $\sigma(\alpha, \theta_t)$ on the flexibility parameter α for tilt angle $\theta_t = 0$ and $\pi/2$ in double logarithmic scales. Other cases of θ_t display similar curves, falling between these two curves. Note that the vertical axis is reduced by using, among other parameters, the total polymer L. An increase in flexibility allows rodlike molecules to make easier accommodation to the interface change, hence we see a reduction of the surface tension. Eventually, as polymers become more flexible in the large α region, the dominating length scale is a, no longer L. Scaled by a instead of L, the surface tension should approach a constant in this limit.[3,10] Going back to the plot in Figure 6 where the vertical axis is scaled by L, the interfacial tension is then linearly dependent on L/a which is α. We indeed see that the interfacial curves increase linearly in the large α limit.

An interesting comparison can be seen between the variation of the interfacial tension in Figure 6 and variation of the magnitude of the change in $C_n - C_i$ in Figure 1C. In general, one would expect that the interfacial tension should be inversely proportional to the interface width. In our case, however, as discussed below the interface width has a monotonic decrease as a function of α in the large α region while the interfacial tension has a completely different trend. In fact, the variation of the interfacial tension is also determined by the magnitude of the change that the interface through; in our case, the change of $C_n - C_i$ is mostly responsible for the change in $\sigma(\alpha, \theta_t)$.
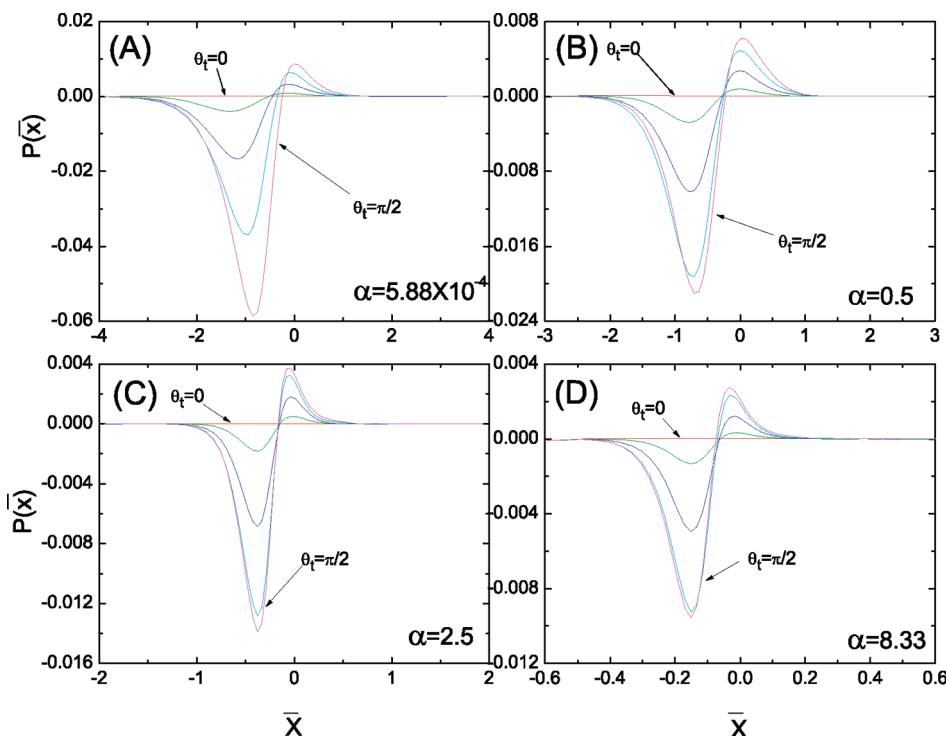
Figure 5. Biaxiality profile $P(\bar{x})$ of the isotropic–nematic interface as a function of $\bar{x} \equiv x/L$ with a few typical values of the tilt angle θ_t for different flexibility of wormlike chains, (A) $\alpha = 5.88 \times 10^{-4}$, (B) $\alpha = 0.5$, (C) $\alpha = 2.5$, and (D) $\alpha = 8.33$. Red, green, blue, cyan, and pink curves represent the tilt angle $\theta_t = 0$, $\pi/9$, $2\pi/9$, $\pi/3$, and $\pi/2$, respectively.
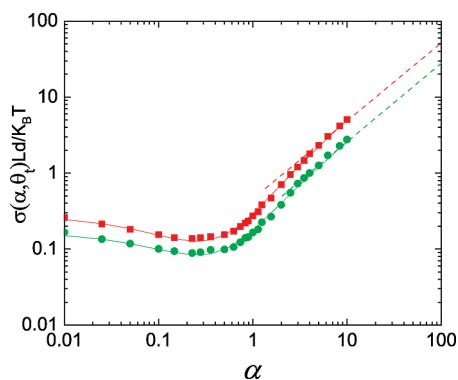

Figure 6. Isotropic–nematic interfacial tension for systems having various degree of flexibility α at tilt angle $\theta_t = 0$ and $\pi/2$ (represented by squares and circles, respectively). Red and green curves are the corresponding fitting results according to eqs 35 to 37. We also added dashed lines $\sigma(\alpha,\theta_t = 0)Ld/k_BT = 0.5635\alpha$ (red) and $\sigma(\alpha,\theta_t = \pi/2)Ld/k_BT = 0.2818\alpha$ (green) in the large α region to indicate the asymptotic behavior.

Another important perspective can be gained from plotting the interfacial tension as a function of $\cos \theta_t$ for typical values of α, shown in Figure 7. We found that for any α the interfacial tension monotonically decreases with the increase of the tilt angle θ_t. This implies that the global free energy minimum can be attained at $\theta_t = \pi/2$, if the nematic director on the far right-hand side is allowed to rotate. The same theoretical conclusion was previously drawn for isotropic–nematic interfaces consisting of rigid-rods[2,5,8] or flexible wormlike chains.[3,6] This observation qualitatively agrees with a recent experimental observation.[13]

We can generally show from an analysis of the functional dependence on θ_t in eq 27 that the interface can only be a function of the variable $\cos^2 \theta_t$. Physically, this reflects the symmetry property, $\sigma(\alpha,\theta_t) = \sigma(\alpha,\pi + \theta_t)$, because of a reflection symmetry against the $z = 0$ plan in Figure 2. Doi and Kuzuu,[8] for example,

even proposed that the interfacial tension for a rod system ($\alpha = 0$) can be approximated by

$$\frac{\sigma(0,\theta_t)Ld}{k_BT} = 0.257(1 + 1.75 \cos^2 \theta_t)^{1/2} \quad (34)$$

which has values higher than our results over the entire region of $\cos \theta_t$ when $\alpha = 0$. A somewhat surprising result from the current calculation is that the dependence of σ in $\cos \theta_t$ is parabolic within the numerical errors and our numerical results can be well captured by a simple empirical formula

$$\frac{\sigma(\alpha,\theta_t)Ld}{k_BT} = A_0(\alpha) \cos^2 \theta_t + B_0(\alpha) \quad (35)$$

which is similar to the Rapini–Papoular model[43] estimating the interfacial tension. The coefficients $A_0(\alpha)$ and $B_0(\alpha)$ were obtained from fitting to the numerical data and can be further represented by

$$A_0(\alpha) = \sum_{m=0}^{3} a_m\alpha^m / \left(1 + \sum_{m=1}^{2} b_m\alpha^m\right) \quad (36)$$

$$B_0(\alpha) = \sum_{m=0}^{3} a_m\alpha^m / \left(1 + \sum_{m=1}^{2} b_m\alpha^m\right) \quad (37)$$

where the constants a_m and b_m are listed in Table 1. This dependence is displayed in Figure 7 as straight lines, where the horizontal axis is $\cos^2 \theta_t$. The dimensionless anchoring strength, i.e., the ratio of the anchoring energy and the interfacial tension as the function of α can be directly calculated from $A_0(\alpha)/B_0(\alpha)$, which is shown in Figure 8 based on eqs 35 to 37 and the fitted coefficients in Table 1. In the rod-like chain limit, $\alpha \to 0$, our calculation shows $A_0(0)/B_0(0) \to 0.58$; in the flexible chain limit,
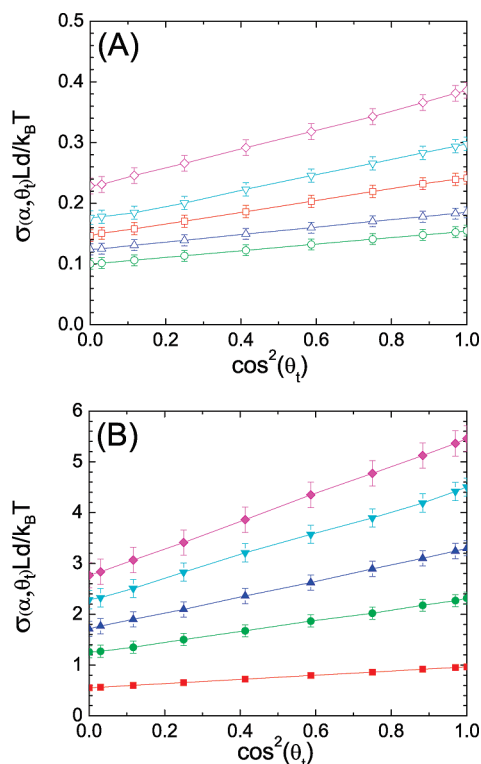
Figure 8. Ratio of the anchoring energy and the interfacial tension for systems having various degree of flexibility α.

Figure 7. Reduced isotropic−nematic interfacial tension defined in eq 33 as a function of the tilt angle θ_t. (A) Open squares, circles, up triangles, down triangles and diamonds represent $\alpha = 0.01, 0.1, 0.5, 1,$ and 1.25, respectively. (B) Filled squares, circles, up triangles and down triangles and diamonds represent $\alpha = 2.5, 5, 6.25, 8.33,$ and 10, respectively.

Table 1. Fitted Coefficients in eqs 35−37

	a_0	a_1	a_2	a_3	b_1	b_2
$A_0(\alpha)$	0.1076	0.4240	0.0721	2.6204	17.710	9.3023
$B_0(\alpha)$	0.1852	1.1654	0.0723	5.0579	17.273	17.948

$\alpha \to \infty$, $A_0(\infty)/B_0(\infty) \to 1.0$; in the vicinity of $\alpha = 0.3$ there is a minimum value of anchoring strength 0.5. Our theoretical prediction on the dimensionless anchoring strength, however, is far smaller than the experimental observation of Puech et al. who studied aqueous dispersions of carbon nanotubes and found the corresponding value is approximately equal to 3.4.[44] So far, the reason for the disagreement is not clear.

The characteristics of the interface can also be examined by interfacial widths measured from the density- and orientational order-parameter profiles as functions of $\bar{x}$. Because of the nonmonotonic variation of these profiles, we have decided to use the second-moment definition,

$$\bar{w} = 2\sqrt{\langle \bar{x}^2 \rangle - \langle \bar{x} \rangle^2} \qquad (38)$$

where the average is evaluated by

$$\langle A(\bar{x}) \rangle = \frac{\int_{-\infty}^{\infty} A(\bar{x}) \left| \dfrac{\mathrm{d}f(\bar{x})}{\mathrm{d}\bar{x}} \right| \mathrm{d}\bar{x}}{\int_{-\infty}^{\infty} \left| \dfrac{\mathrm{d}f(\bar{x})}{\mathrm{d}\bar{x}} \right| \mathrm{d}\bar{x}} \qquad (39)$$

with the function $f(\bar{x})$ being $C\bar{\phi}(\bar{x})$ for the density interfacial width or $S(\bar{x})$ for the orientational interfacial width.

The interface widths $w_\phi(\alpha, \theta_t)$ calculated from the profile of segmental density and $w_S(\alpha, \theta_t)$ from order parameter for $\theta_t = 0$
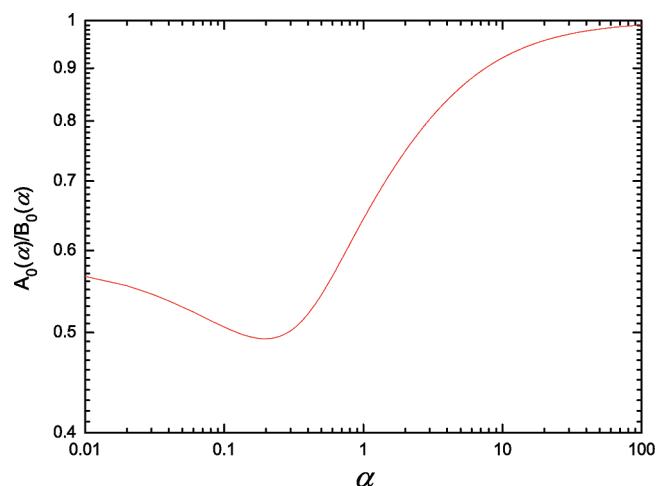
(squares) and $\pi/2$ (circles) are displayed in Figure 9. Other values of θ_t give a rise to curves in between these two. In both $\bar{w}_\phi \equiv w_\phi/L$ and $\bar{w}_S \equiv w_S/L$, the interfacial widths decrease with an increase in α. Those systems with $\theta_t = 0$ have a broader interface width than those with $\theta_t = \pi/2$, for a fixed α; this result is consistent with earlier studies.[2,3,6] In the small α regime, the interface width has a sharp drop with the increase of α. In the large α region, we anticipate that the interface width is predominantly controlled by the Kuhn length a, $w \sim a$. Reflected in these plots where w is scaled by L, we see an $1/\alpha$ behavior in the large α region.

As demonstrated in Appendix A, in the limit of $\alpha \ll 1$, the general formalism developed for the wormlike isotropic−nematic interface in this work exactly recovers that of the interface problem of rigid rods, originally developed by Onsager for the bulk phase,[19] and later generalized by others for the description of the interfacial problem.[1,2,9]

In Figure 10, we display the interfacial tension previously found in this limiting case. Both results by Doi-Kuzuu[8] and McMullen[1] can be seen far above the results found in the current work (filled circles); this is caused by the trial density functions used in these theoretical approaches. The result[2] from a numerical treatment of the Onsager problem, without the explicit consideration of the biaxiality, given in the plot as squares, is also above this calculation and cannot be represented by the quadratic function in $\cos \theta_t$; neglecting biaxiality is probably the cause of this deviation.

In the flexible-chain limit, $L \gg a$, the formalism developed in this work also recovers those used by Cui, Akcakir and Chen,[3] who have studied the isotropic−nematic interface formed by long wormlike polymers. In this limit the characteristic length scale is a and we can show that the reduced surface tension $\sigma ad/k_BT$ approaches a constant. In Figure 11, we plot the data obtained from the current work for $\alpha = 10$, which can be compared with the projected $\alpha \gg 1$ result, taken from eqs 35 to 37 in the large α limit. It is not clear where the discrepancy between the result in ref 3 and our current calculation comes from, seen in this plot.

Chen, Sato, and Teramoto measured the surface tension of polysaccharide molecule as a function of molecular weight M, which can be translated into contour length L in this model. The molecules in these systems can be considered almost rigid. It is interesting to note that their measurement gives a σM that decreases as M increases, which is consistent with the qualitative feature of $\sigma Ld/k_BT$ in the small L/a region, found in this work. Later, Chen and Gray measured the interfacial tension[45] in the system of aqueous suspensions of cellulose crystallites through changing crystallites concentration and obtained the relatively satisfactory
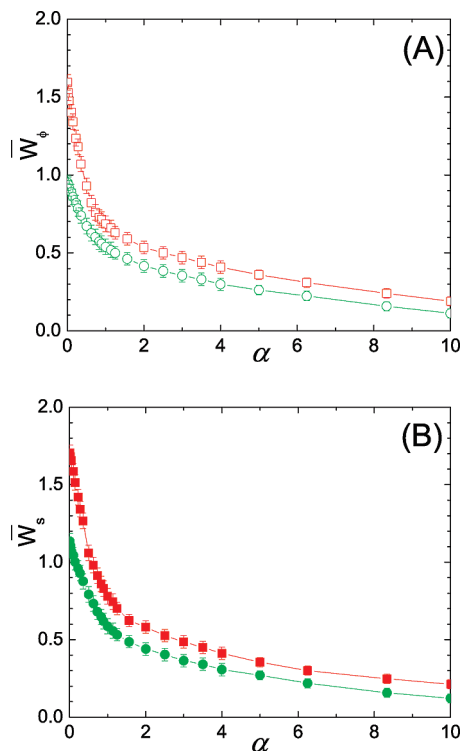
Figure 9. Reduced interface width $\overline{w} \equiv w/L$ defined in eq 38 for systems with various flexibility α at two tilt angles, $\theta_t = 0$ (squares) and $\pi/2$ (circles). $\overline{w}_\phi$ (A) and $\overline{w}_S$ (B) represent the interfacial widths calculated from the density and order parameter profiles, respectively.
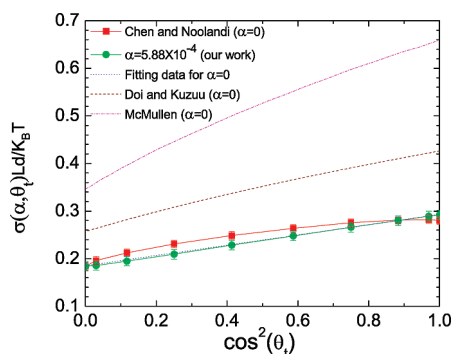

Figure 10. Interfacial tension for different tilt angles θ_t in the rod-like chain limit $\alpha \ll 1$. The curve going through squares was obtained by Chen and Noolandi,[2] whose results almost overlaps with those of van der Schoot.[18] The curve going through circles represents our calculated results for $\alpha = 5.88 \times 10^{-4}$. The dotted curve was extrapolated from eqs 35 to 37, by setting $\alpha = 0$. The dashed curve was obtained by Doi and Kuzuu.[8] The dash-dotted curve was obtained by McMullen.[1]

results compared to theoretical predictions[1,2] after considering the equivalent hard-core diameters of the rod-like particles. The theoretical results[1,2,8,9] on the prediction of interfacial tension $\sigma Ld/k_BT$ for $L \ll a$, however, are usually far lower than other experimental observations.[13,45] It is not clear whether we can ascribe the discrepancy to the flexibility on the polymer chain, to the polydispersity in molecular weight, to the soft attractive interactions between the polysaccharide molecules,[13] or the definition of the effective diameter[45] of a polymer segment in the experiment.

4. Summary

In this work, we calculated the interfacial properties of the isotropic−nematic interface from a model that contains the Onsager interaction for the description of the orientational-
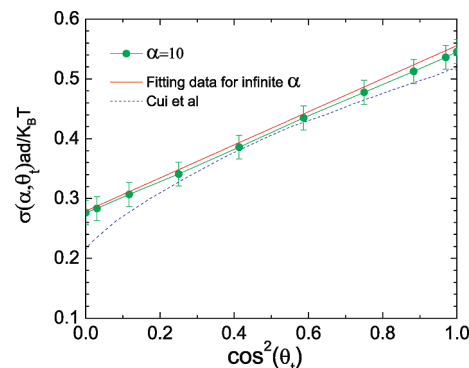

Figure 11. Interfacial tension for different tilt angles θ_t in the flexible chain limit, $\alpha \gg 1$. The curve with circles represents our result for $\alpha = 10$, and the solid curve is an extrapolation from eqs 35 to 37 by taking $\alpha \rightarrow \infty$. The dashed curve was obtained by Cui, Akcakir, and Chen.[3]

dependent interaction and the wormlike-chain statistics for the description of the flexibility of chains. We particularly paid attention to the flexibility dependence, connecting to interfacial properties previously studied in two limits: rods and flexible chains. One particularly interesting case is that the reduced surface tension, $\sigma Ld/k_BT$, where L and d are the polymer's total contour length and excluded-volume diameter, decreases as a rigid chain is softened, goes through a minimum, and then increases linearly in the flexible limit shown in Figure 6. This decrease near the rigid region qualitatively explains a recent experimental observation.[13]

We have also verified that the general trend of the tilt-angle dependence in a lyotropic isotropic−nematic interface, reflected by the surface tension and seen previously in rod- and flexible-chain models, is also valid in the semiflexible case, shown in Figure 7. Weak biaxialities have been found in all systems considered in this work, consistent with those seen in models describing these two limits.

We described the usage of the software package SPHEREPACK in treating the orientational dependence of the physical properties in this system. This method can be easily adopted for related wormlike-polymer problems, that requires the numerical solution to a modified differential equation with both positional and orientational dependencies.

Appendix A: The Rod Limit: $\alpha = L/a \ll 1$

In this Appendix, we show that the formalism given in section 2 is identical to the Onsager model for a liquid-crystal interface in the limit of $a \gg L$. The modified diffusion equation, eq 8, can be reduced to

$$\frac{\partial}{\partial s} q(\mathbf{r}, \mathbf{u}, s) = \left[-\mathbf{u} \cdot \nabla - \frac{1}{a} W(\mathbf{r}, \mathbf{u}) \right] q(\mathbf{r}, \mathbf{u}, s) \qquad (40)$$

By directly taking the derivative, we can show that eq 40 can be formally solved

$$q(\mathbf{r}, \mathbf{u}, s) = \exp\left\{ -\frac{1}{a} \int_0^s W(\mathbf{r} - s'\mathbf{u}, \mathbf{u}) \, ds' \right\} \qquad (41)$$

We can then write the density of segments, labeled s along rods

$$\phi(\mathbf{r}, \mathbf{u}, s) = \frac{n}{4\pi VaQ} \int_0^L ds \, q(\mathbf{r}, \mathbf{u}, s) q(\mathbf{r}, -\mathbf{u}, L - s)$$

$$= \frac{nL}{4\pi VaQ} \exp\left[-\frac{1}{a} \int_0^L W(\mathbf{r} + s'\mathbf{u} - s\mathbf{u}, \mathbf{u}) \, ds' \right] \qquad (42)$$

which satisfies the normalization condition $\int d\mathbf{r}\, d\mathbf{u}\, \phi(\mathbf{r},\mathbf{u},s) = nL/a$. In the above the partition function of a single chain reads

$$Q = \frac{1}{4\pi V} \int d\mathbf{r}\, d\mathbf{u} \exp\left[-\frac{1}{a} \int_0^L W(\mathbf{r},\mathbf{u})\, ds \right] \quad (43)$$

The above solution of $\phi(\mathbf{r},\mathbf{u},s)$ has the mathematical property,

$$\phi[\mathbf{r} - \mathbf{u}(L/2 - s), \mathbf{u}, s] = \phi(\mathbf{r}, \mathbf{u}, L/2)$$

which is valid for rod-like molecules only.

There are three terms in the free energy, eq 6. The last term on the right-hand side can be expressed as

$$\text{last term} = -\frac{1}{n} \int d\mathbf{r}\, d\mathbf{u}\, W(\mathbf{r},\mathbf{u})\phi(\mathbf{r},\mathbf{u})$$

$$= -\frac{1}{nL} \int_0^L ds \int d\mathbf{r}\, d\mathbf{u}\, W(\mathbf{r},\mathbf{u})\phi(\mathbf{r},\mathbf{u},s)$$

$$= -\frac{1}{nL} \int_0^L ds \int d\mathbf{r}\, d\mathbf{u}\, W(\mathbf{r}+s\mathbf{u}-L\mathbf{u}/2,\mathbf{u})\phi(\mathbf{r},\mathbf{u},L/2)$$

$$(44)$$

On the basis of eq 42, we have

$$\text{last term} = \frac{a}{nL} \int d\mathbf{r}\, d\mathbf{u}\, \phi(\mathbf{r},\mathbf{u},L/2) \ln \phi(\mathbf{r},\mathbf{u},L/2) - \ln\left(\frac{n}{Q}\right)$$

$$- \ln\left(\frac{L}{4\pi Va}\right) \quad (45)$$

The excluded-volume interaction term in eq 6 can also be written as

$$\frac{a^2 d}{nL^2} \int ds\, ds'\, d\mathbf{r}\, d\mathbf{r}'\, d\mathbf{u}\, d\mathbf{u}'\, \phi(\mathbf{r},\mathbf{u},s)\phi(\mathbf{r}',\mathbf{u}',s')|\mathbf{u}$$

$$\times \mathbf{u}'|\delta(\mathbf{r}-\mathbf{r}') = \frac{a^2 d}{nL^2} \int ds\, ds'$$

$$\times \int d\mathbf{r}\, d\mathbf{r}'\, d\mathbf{u}\, d\mathbf{u}'\, \phi(\mathbf{r},\mathbf{u},L/2)\phi(\mathbf{r}',\mathbf{u}',L/2)|\mathbf{u}$$

$$\times \mathbf{u}'|\delta(\mathbf{r}+s\mathbf{u}-L\mathbf{u}/2, \mathbf{r}'+s'\mathbf{u}'-L\mathbf{u}'/2) \quad (46)$$

Instead of $\phi(\mathbf{r},\mathbf{u},L/2)$, we can introduce the number density of rods, represented by the center of mass of each rod, $\rho(\mathbf{r},\mathbf{u}) \equiv (a/L)\phi(\mathbf{r},\mathbf{u},L/2)$, the Helmholtz free energy of the entire system can then be written as

$$\frac{nF}{k_B T} = \int d\mathbf{r}\, d\mathbf{u}\, \rho(\mathbf{r},\mathbf{u}) \ln \rho(\mathbf{r},\mathbf{u})$$

$$+ \frac{1}{2} \int d\mathbf{r}\, d\mathbf{r}'\, d\mathbf{u}\, d\mathbf{u}'\, \rho(\mathbf{r},\mathbf{u})\rho(\mathbf{r}',\mathbf{u}')(2d)|\mathbf{u}\times\mathbf{u}'|\omega(\mathbf{r},\mathbf{r}',\mathbf{u},\mathbf{u}')$$

$$(47)$$

where $\omega(\mathbf{r},\mathbf{r}',\mathbf{u},\mathbf{u}') \equiv \int ds\, ds'\, \delta(\mathbf{r}+s\mathbf{u}-L\mathbf{u}/2,\mathbf{r}'+s'\mathbf{u}-L\mathbf{u}'/2)$, within a trivial $\ln(L/4\pi Va)$ constant shift. The above free energy is the starting point of the model considered in refs 1, 2, 5, 8, 9, and 18. Note that the Kuhn length a disappears completely in eq 47.

Appendix B: The Flexible Chain Limit: $\alpha = L/a \gg 1$

In this Appendix, we show that the formalism given in section 22 is identical to the free energy model for a liquid-crystal interface formed by lytropic polymers, in the limit of $L \gg a$. One important fact is such that in order to reach the isotropic−nematic transition point, the segmental density[20,22,41] can be estimated to have the order of magnitude

$$\frac{nL}{Va} \sim \frac{1}{a^2 d} \quad (48)$$

hence $n^{-1} \sim (L/a)(a^2 d/V)$. Using this estimate, we can show that the second and third terms of eq 6 have an order of magnitude of L/a, much greater than the $\ln(L/a)$-order of the $\ln(n/Q)$ term in eq 6. The latter can thus be dropped in the limit $L \gg a$. The grand thermodynamic potential for the system can then be written as

$$\frac{\Xi}{k_B T} = -\int d\mathbf{r}\, d\mathbf{u}\, W(\mathbf{r},\mathbf{u})\phi(\mathbf{r},\mathbf{u}) + a^2 d \int d\mathbf{r}\, d\mathbf{u}\, d\mathbf{u}'\, \phi(\mathbf{r},\mathbf{u})|\mathbf{u}$$

$$\times \mathbf{u}'|\phi(\mathbf{r},\mathbf{u}') - \frac{a\bar{\mu}}{L} \int d\mathbf{r}\, d\mathbf{u}\, \phi(\mathbf{r},\mathbf{u})$$

$$(49)$$

where $\bar{\mu} \equiv \mu/k_B T$ is the chemical potential per chain.

In the long-chain limit, $q(\mathbf{r},\mathbf{u},s)$ becomes s-independent in most region of s,

$$q(\mathbf{r},\mathbf{u},s) \sim \tilde{q}(\mathbf{r},\mathbf{u}) \quad (50)$$

According to eq 8, we can then consider a solution to

$$[\nabla_\mathbf{u}^2 - a\mathbf{u}\cdot\nabla - W(\mathbf{r},\mathbf{u})]\tilde{q}(\mathbf{r},\mathbf{u}) = 0 \quad (51)$$

Note that $\phi(\mathbf{r},\mathbf{u})$ is related to $\tilde{q}(\mathbf{r},\mathbf{u})$ by

$$\phi(\mathbf{r},\mathbf{u}) \propto \tilde{q}(\mathbf{r},\mathbf{u})\tilde{q}(\mathbf{r},-\mathbf{u}) \quad (52)$$

up to a proportional coefficient.

Equations 49, 51, and 52 are identical to eqs 1, 4, and 6 in ref 24 for the segmental density $\phi(\mathbf{r},\mathbf{u})$, which was denoted as $\rho(\mathbf{x},\mathbf{u})$ in ref 24. Introducing a chain density $\rho_c(\mathbf{x},\mathbf{u}) = (a/L)\phi(\mathbf{r},\mathbf{u})$ and $\overline{W}(\mathbf{r},\mathbf{u}) = (L/a)W(\mathbf{r},\mathbf{u})$, we can also show that eqs 49, 51 and 52 are the same as the starting eqs 1−3 in ref 3, except for a misprint of factor $1/2$ in eq 2 of ref 3 introduced in the write-up stage while the original calculation was performed correctly with no such factor.

References and Notes

(1) McMullen, W. E. *Phys. Rev. A* **1988**, *38*, 6384.
(2) Chen, Z. Y.; Noolandi, J. *Phys. Rev. A* **1992**, *45*, 2389.
(3) Cui, S. M.; Akcakir, O.; Chen, Z. Y. *Phys. Rev. E* **1995**, *51*, 4548.
(4) Al-Barwani, M. S.; Allen, M. P. *Phys. Rev. E* **2000**, *62*, 6706.
(5) Shundyak, K.; van Roij, R. *J. Phys.: Condens. Matter* **2001**, *13*, 4789.
(6) Drovetsky, B. Y.; Liu, A. J.; Mak, C. H. *J. Chem. Phys.* **1999**, *111*, 4334.
(7) Koch, D. L.; Harlen, O. G. *Macromolecules* **1999**, *32*, 219.
(8) Doi, M.; Kuzuu, N. *J. Appl. Polym. Sci., Polym. Symp.* **1985**, *41*, 65.
(9) Chen, Z. Y. *Phys. Rev. E* **1993**, *47*, 3765.
(10) Grosberg, A. Y.; Pachomov, D. V. *Liq. Cryst.* **1991**, *10*, 539.
(11) Holyst, R.; Poniewierski, A. *Phys. Rev. A* **1988**, *38*, 1527.
(12) Chen, W. L.; Sato, T.; Teramoto, A. *Macromolecules* **1996**, *29*, 4283.
(13) Chen, W. L.; Sato, T.; Teramoto, A. *Macromolecules* **1999**, *32*, 1549.

(14) Viamontes, J.; Oakes, P. W.; Tang, J. X. *Phys. Rev. Lett.* **2006**, *97*, 118103.
(15) Oakes, P. W.; Viamontes, J.; Tang, J. X. *Phys. Rev. E* **2007**, *75*, 061902.
(16) Dogic, Z.; Fraden, S. *Langmuir* **2000**, *16*, 7820.
(17) Dogic, Z.; Purdy, K. R.; Grelet, E.; Adams, M.; Fraden, S. *Phys. Rev. E* **2004**, *69*, 051702.
(18) van der Schoot, P. *J. Phys. Chem. B* **1999**, *103*, 8804.
(19) Onsager, L. *Ann. N. Y. Acad. Sci.* **1949**, *51*, 627.
(20) Khokhlov, A. R.; Semenov, A. N. *Physica* **1982**, *112*, 605.
(21) Grosberg, A. *Theoretical and Mathematical Models in Polymer Research: Modern Methods in Polymer Research and Technology (Polymers, Interfaces and Biomaterials)*; Academic Press: Boston, MA, 1998.
(22) Chen, Z. Y. *Macromolecules* **1993**, *26*, 3419.
(23) Duchs, D.; Sullivan, D. E. *J. Phys.: Condens. Matter* **2002**, *14*, 12189.
(24) Chen, J. Z. Y.; Sullivan, D. E. *Macromolecules* **2006**, *39*, 7769.
(25) Chen, J. Z. Y.; Sullivan, D. E.; Yuan, X. Q. *Macromolecules* **2007**, *40*, 1187.
(26) Deng, M. G.; Jiang, Y.; Liang, H. J.; Chen, J. Z. Y. *J. Chem. Phys.* **2010**, *133*, 034902.
(27) Matsen, M. W. *J. Chem. Phys.* **1996**, *104*, 7758.
(28) Song, W. D.; Tang, P.; Zhang, H. D.; Yang, Y. L.; Shi, A. C. *Macromolecules* **2009**, *42*, 6300.
(29) Adams, J. C.; Swarztrauber, P. N. *Computer code SPHEREPACK 3.2,* **2009**; http://www.cisl.ucar.edu/css/software/spherepack/.
(30) Saito, N.; Takahashi, K.; Yunoki, Y. *J. Phys. Soc. Jpn.* **1967**, *22*, 219.
(31) Kratky, O.; Porod, G. *Recl. Trav. Chim.* **1949**, *68*, 1106.
(32) Fredrickson, G. H. *The Equilibrium Theory of Inhomogeneous Polymers*; Clarendon: Oxford, U.K., 2006.
(33) Deng, M. G.; Jiang, Y.; Liang, H. J.; Chen, J. Z. Y. *Macromolecules* **2010**, *43*, 3455.
(34) Odijk, T. *Macromolecules* **1986**, *19*, 2313.
(35) Lekkerkerker, H. N. W.; Coulon, P.; van der Haegen, R.; Deblieck, R. *J. Chem. Phys.* **1984**, *80*, 3427.
(36) Press, W. H.; Teukolsky, S. A.; Vetterling, W. T.; Flannary, B. P. *Numerical Recipes in C*, 2nd ed.; Cambridge University Press: Cambridge, U.K., 1992.
(37) Chantawansri, T. L.; Bosse, A. W.; Hexemer, A.; Ceniceros, H. D.; Garcia-Cervera, C. J.; Kramer, E. J.; Fredrickson, G. H. *Phys. Rev. E* **2007**, *75*, 031802.
(38) Swarztrauber, P. N. *Mon. Weather Rev.* **1993**, *121*, 3415.
(39) Swarztrauber, P. N. *J. Comput. Phys.* **2000**, *159*, 213.
(40) Gradshteyn, I. S.; Ryzhik, I. M. *Tables of Integrals, Series, and Products*; Academic: New York, 1980.
(41) Vroege, G. J.; Odijk, T. *Macromolecules* **1988**, *21*, 2848.
(42) de Gennes, P. G. *The Physics of Liquid Crystals*, 2nd ed.; Clarendon: Oxford, U.K., 1993.
(43) Rapini, A.; Papoular, M. J. *J. Phys. (Paris), Colloq.* **1969**, *30*, C4–54.
(44) Puech, N.; Grelet, E.; Poulin, P.; Blanc, C.; van der Schoot, P. *Phys. Rev. E* **2010**, *82*, 020702(R).
(45) Chen, W.; Gray, D. G. *Langmuir* **2002**, *18*, 633.